The current issue and full text archive of this journal is available at
www.emeraldinsight.com/0961-5539.htm

Effect of computational grid in industrial-scale boiler modeling

A. Saario and A. Oksanen
Institute of Energy and Process Engineering, Tampere University of Technology, Tampere, Finland

Received 14 November 2006
Revised 10 September 2007
Accepted 13 December 2007

Abstract

Purpose – The purpose of this paper is to study the effect of a computational grid in computational fluid dynamics-based mathematical modeling, focusing on but not limiting the attention to industrial-scale boilers.

Design/methodology/approach – A full boiler model is used to show the difficulties related to judging iteration and discretization errors in boiler modeling. Then, a single jet is studied in detail to determine the proper degree of local grid refinement required in the vicinity of jets in the full boiler model. Both a nonreactive axisymmetric jet exhausting into a quiescent atmosphere and a reactive jet exhausting into a crossflow are studied.

Findings – Over two million computational cells are required for the grid-independent solution for a single jet. Local grid refinement is shown to be a good option for improving the results consistently without an excessive increase in the number of computational cells. Using relatively coarse grids of tetrahedral cells with a finite-volume-based solver may cause serious errors in results, typically by overpredicting the jet spreading rate and underpredicting the mean axial centerline velocity. Relatively coarse grids of hexahedral cells are less prone to error in a case where a jet exhausts into a quiescent atmosphere. However, their performance deteriorates when a crossflow is introduced. As assumed, the differences in the predicted reaction rate and species concentrations are significant in the reactive case. It is confirmed that the standard k-ε model tends to overpredict the axisymmetric jet spreading rate. The estimated inlet turbulence intensity is not among the most critical factors in modeling. Estimations of the axisymmetric jet centerline velocity from the analytical correlation may not coincide with the modeling results.

Practical implications – The error caused by the computational grid may easily dominate the errors caused by simplifying models used in industrial-scale boiler modeling (turbulence, combustion, radiative heat transfer, etc.).

Originality/value – The present study deals with grid independency issues in industrial-scale boiler modeling in a systematic and profound manner.

Keywords Combustion, Fluid dynamics, Turbulence, Mathematical modelling, Boilers, Jets

Paper type Research paper

1. Introduction

The computational grid is one of the most important factors affecting the accuracy of computational fluid dynamics (CFD) modeling. It can be argued that due to the lack of sufficient computational capacity the grids nowadays used to describe industrial-scale boilers are always too coarse, which further stresses the importance of a good quality grid. Nevertheless, the computational grid has not always received the attention it deserves in the industrial-scale boiler modeling community. In fact, in many studies grid independency has not been assessed at all, or it has been assessed nonsystematically or in insufficient detail. Moreover, in some studies the conclusion "reasonably grid-independent solution" has been drawn somewhat hastily.

International Journal of Numerical Methods for Heat & Fluid Flow
Vol. 19 No. 1, 2009
pp. 93-117

0961-5539
DOI 10.1108/09615530910922189

According to Ferziger and Peric (1999, p. 331), many tests intended to determine model validity have proven inconclusive because the numerical errors were greater than the effects of the model. Lockwood *et al.* (2001, p. 5) point out that the worst predictive discrepancies in combustion modeling are often due to numerical inaccuracies, although it is fashionable to put all the blame on the submodels. The scarcity of grid independency studies is probably due to the additional work and computer time required for performing the grid independency analysis. The boiler geometries are typically highly complex, and building a good-quality grid can be an extremely laborious task.

When the effect of grid refinement has been studied at least in some detail, it has been shown to affect results significantly (Hill and Smoot, 2000; Gillis and Smith, 1990; Coelho and Carvalho, 1996; Weber *et al.*, 1993; Stopford, 2002; Pokela and Huttunen, 2005). Hill and Smoot (2000, p. 450) showed significant discrepancies in predicted nitric oxide profiles in an industrial-scale coal-fired boiler between two grids with 192,000 and 337,000 computational cells. At most locations the predictions based on the finer grid agreed better with the experimental data. Gillis and Smith (1990) concluded that more than 250,000 cells are required to obtain grid independency in complex industrial furnace flows. Weber *et al.* (1993) demonstrate the necessity of applying dense grids if turbulence models are to be assessed. According to Pokela and Huttunen (2005), the number of tetrahedral cells required is approximately twice the number of hexahedral cells necessary to obtain the same accuracy in boiler modeling. Karvinen and Ahlstedt (2005) observed the same trend for a single jet in crossflow. They also showed that to achieve strict grid independency of all variables in their case requires several hundreds of thousands of cells. Karvinen *et al.* (2006) showed that frequently grid densities typical of industrial boiler modeling are not sufficient. Weber *et al.* (1993) and Karvinen *et al.* (2006) both conclude that with the grid densities used in industrial boilers the grid refinement is more essential for results than the turbulence model used.

2. Computational errors

The iteration error is the difference between the exact and the iterative solutions of the discretized equations. The truncation error of the Taylor series expansion acts as a source of the discretization error, which is the difference between the exact solution of the mathematical model and the exact solution of the discretized equations. The modeling error is the difference between the real flow and the exact solution of the mathematical model. When validating the CFD results, the errors should be estimated starting from the iteration error, then the discretization error should be studied, and finally the modeling error (Ferziger and Peric, 1999; Casey and Wintergerste, 2000). The iteration and discretization errors should be small compared to the experimental uncertainty, because this is the only way that the effect of a model or of boundary conditions on the results can be assessed (Ferziger and Peric, 1999, p. 322).

The quality of the grid affects both the accuracy and the convergence rate of the solution (Ferziger and Peric, 1999; White, 2006). In particular, highly distorted computational cells may seriously impede convergence (Lockwood *et al.*, 2001; Casey and Wintergerste, 2000). The accuracy of finite-volume methods is improved when the line connecting two neighboring control volume centers firstly passes through the center of the common face and secondly is orthogonal to the common face (Ferziger and Peric, 1999). If the flow is oblique to the grid, numerical error increases, and peaks or rapid variations in the variables will be smoothed out. The use of hexahedral cells is

attractive because the grid lines may be kept at least partially aligned with streamlines, thus reducing numerical error, whereas with tetrahedral cells no organized grid line directions exist. Dispersion (diffusion) errors dominate in the convective transport equations, whereas amplitude errors are significant in the diffusive transport equations. These sources of errors are discussed in more detail, e.g. in Chung (2002).

3. Turbulent jets and computational fluid dynamics

The mixing of jets is one of the most important factors affecting combustion efficiency and emissions in industrial-scale boilers. For example, with the commonly used nitric oxide reduction method, called selective noncatalytic reduction (Miller and Bowman, 1989), the ammonia jets should provide a sufficient depth of penetration into the boiler bulk flow and a good mixing with combustion products. These factors can be controlled by jet parameters such as jet diameter, momentum, injection location, number of jets, and nozzle design (Weber *et al.*, 1998). In the following, a brief summary of turbulent axisymmetric jets is provided.

After the initial development region, turbulent axisymmetric jets exhausting into a quiescent atmosphere reach self-similarity, spreading and decaying linearly in the downstream direction. The mean velocity becomes self-similar approximately at $x/d = 20$ (White, 2006, p. 479) or at $x/d = 30$ (Pope, 2000, p. 98), where x is the axial distance from the jet inlet and d is the jet inlet diameter. The turbulence components take longer to develop; turbulent fluctuations become self-similar at $x/d = 50$-70, and isotropic turbulence is not yet reached even at $x/d = 100$ (White, 2006, p. 479). The mean velocity profile and the spreading rate are traditionally assumed independent of Reynolds number, *Re*, whereas the small-scale turbulent structures become smaller at larger *Re*. Surrounding fluid is entrained into the jet during the bursts of turbulent activity at the edge of the jet.

An analytical solution for the axisymmetric jet centerline velocity, u_c, can be written in the isothermal case as (Hussein *et al.*, 1994; Panchapakesan and Lumley, 1993; White, 2006; Pope, 2000):

$$\frac{u_c(x)}{u_0} = \frac{Bd}{x - x_0}, \tag{1}$$

where u_0, d, B, and x_0 are the velocity at the jet inlet, the jet inlet diameter, an experimental velocity-decay constant, and the virtual origin (the point from which the self-similar region seems to grow, see, e.g. White (2006, p. 475)), respectively.

The standard k-ε model is known to overpredict the round jet spreading rate by 25-40 percent (Wilcox, 1998, p. 137). Modifications have been suggested in the literature to remove round jet anomaly from the standard k-ε model, one of the which is the model of Shih *et al.* (1995) used in the present study. This model has been shown to be superior to the standard k-ε model in round jet predictions (Shih *et al.*, 1995), but it has also been shown not to be superior to the standard k-ε model in the case of round jet in crossflow (Karvinen and Ahlstedt, 2005).

When a jet penetrates into crossflow instead of quiescent atmosphere, very complex flow structures will develop, see, e.g. Andreopoulos and Rodi (1984). Weber *et al.* (1998) studied the penetration and mixing of reburn jets in boilers. They showed that the discrepancy between the available jet trajectory correlations is great for a jet in crossflow, and the predictions are strongly dependent on the conditions in question.

Weber *et al.* (1998) also showed that the penetration depth of each jet is sensitive to local flow conditions prevailing upstream of the injection position, and thus a good knowledge of the overall flow pattern is required within the boiler.

4. Description of modeled cases and grid refinement

First, a full boiler geometry is studied in order to show the difficulties related to judging the iteration and discretization errors in boiler modeling. In the second stage, a single jet is studied in considerable detail to discover the required degree of local grid refinement (solution-adaptive gridding) for the full boiler grid.

In the present study, small ammonia injection jets applied in the selective noncatalytic reduction are subjected to examination. It must be realized that there is a huge discrepancy in scale between the small jets (inlet diameter $d = 42.5$ mm) and the full boiler (depth 6 m, width 8 m, height 18 m) and that there may be up to 20 ammonia injections in a real boiler, the facts which limit the increase in the number of cells that can be feasible per one jet. Both grids consisting of hexahedral (six faces and eight vertices) and of tetrahedral (four faces and four vertices) cells are applied in order to compare their performances. All the cases are modeled in 3D.

4.1 Full boiler

Four grids of hexahedral cells of a full boiler geometry are studied in a reactive flow case. The boiler studied is a bubbling fluidized bed boiler. A detailed description of the case and boundary conditions can be found elsewhere (Saario and Oksanen, 2007).

4.1.1 Grid refinement in full boiler. Grid nodes in each direction should be in principle doubled in a grid refinement study. However, a reasonable study can be performed with a lesser increment; it has been suggested that 50 percent (Ferziger and Peric, 1999, p. 316) or even only 10 percent (Roache, 1994, p. 409) more nodes in each direction than in the original grid is sufficient. If the grid is not refined sufficiently, the results of a grid refinement study may be obscured by other error sources, such as iterative error or machine round-off error (Roache, 1994).

In the full boiler study, a grid with approximately 100,000 hexahedral cells is systematically refined three times, resulting in four different grids of hexahedral cells which are summarized in Table I.

The computational grid of a full boiler consisting of 256,654 cells and an enlargement of the vicinity of a single ammonia jet are shown in Figure 1. The grid is built somewhat denser near the ammonia jets. The area downstream of the boiler bull-nose level does not affect the results significantly, and hence larger computational cells are used there. Attention is paid to keeping the cell edge ratio (maximum edge length/minimum edge length) reasonably small, as well as to changing the grid spacing continuously. At every step the grid is refined by approximately 25 percent in each direction. The grid topology and the relative spatial density of grid points are

Table I. Grids of hexahedral cells used in full boiler modeling

Grid of hexahedral cells	Total number of cells
Very coarse	100,857
Coarse	256,654
Medium	543,719
Dense	1,083,117

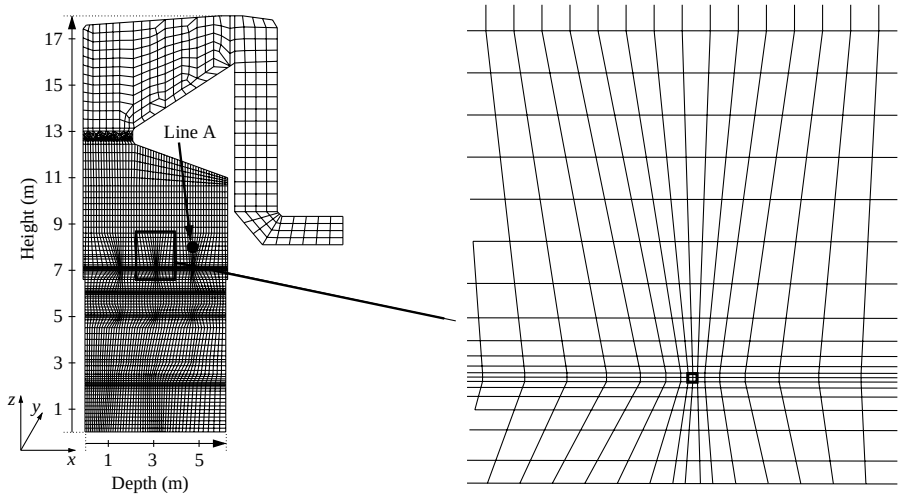

(a) Full boiler geometry (256,654 cells). Line A Penetrates into paper

(b) Enlargement of single ammonia injection (256,654 cells)

Figure 1. Computational grid in full boiler model

retained as unchanged as possible on all the grid levels. Creating these four different good-quality grids consisting of hexahedral cells throughout the boiler required a considerable amount of work. In contrast, the generation of grids consisting of tetrahedral cells is easy to automate, which is one of the reasons for their popularity.

4.2 Nonreactive axisymmetric jet exhausting into quiescent atmosphere

A single axisymmetric jet exhausting into a quiescent isothermal ($T = 440$ K) atmosphere is studied. The inlet velocity of the jet is high, $u_0 = 115$ m/s, and *Re* is of order 140,000. The jet momentum is kept constant with respect to the case with the full boiler. It is reasonable to assume that the same grid resolution and the use of the same models will produce similar discretization and modeling errors in both the single jet case and the full boiler case.

A large rectangular enclosure ($12 \times 6 \times 6$ m) is modeled to study the single jet. To exclude the effect of boundaries, only the side of the rectangular volume that the jet comes from is defined as a wall, whereas all the other sides are defined as open outlets with a specified pressure. Most of the computational cells are placed in the vicinity of the jet inlet and following the direction of axisymmetric jet penetration and consequently towards the outer part the enclosure is covered with a coarse grid. In the vicinity of the ammonia jet, the baseline single jet grid of hexahedral cells is built to closely resemble the full boiler grid with 256,654 cells. The jet inlet pipe is not modeled, but a plug-flow type velocity profile is provided at the inlet. In order to be able to build a good-quality grid using hexahedral cells, the real round jet inlets are replaced by square inlets in all grids used in the present study. These simplifications do not affect the overall outcome of the grid dependency study. The dimensions of square inlets are chosen such that the jet momentum remains unaltered. The findings of the present study show that the jet velocity contours are almost fully axisymmetric already at

$x/d = 5$ (x is the axial distance from the jet inlet and d is the jet inlet diameter) regardless of the square inlet approximation.

4.2.1 Local grid refinement in nonreactive axisymmetric jet. It is important to refine the grid where the gradients of solved quantities are large and where the reactions take place, such as in jet shear layers. Here, the local grid refinement is based either on the magnitude of turbulence kinetic energy or on the gradient of velocity magnitude. The grids of hexahedral cells are locally refined by applying nonconformal adaption which subdivides each cell isotropically, allowing "hanging" nodes, see Chung (2002) and Murthy and Mathur (2001). Refining a single 3D hexahedral cell results in seven new cells, i.e. eight cells are created in total. The number of cells is increased by 3,444 between successive refinements. This rather low number is understandable, keeping in mind that we must apply the corresponding refinement for all jets in the full boiler model. For the same reason, the jet inlet was represented by only four cells in the baseline grid of hexahedral cells. The number of cells at the inlet increases quickly when the grids are refined. The grids of hexahedral cells used in a single jet refinement study are summarized in Table II, and a few of them are shown in Figure 2(a)-2(c).

Table III summarizes the properties of the differently generated grids of tetrahedral cells, and grid I of tetrahedral cells is shown in Figure 2(d). All grids of tetrahedral cells are built by creating first a straight line along the axisymmetric jet centerline from which the cell size is gradually increased in the radial direction (Figure 2(d) and Table III).

Finally, the single jet cases are calculated also with extremely dense grids, using both grids of hexahedral and tetrahedral cells (Tables II and III).

4.3 Reactive jet exhausting into crossflow

Since the ammonia jets in a real boiler encounter a hot crossflow, a few cases corresponding to such conditions are studied as well. The case description in Section 4.2 applies to the crossflow case also, unless stated otherwise in the present section. The velocity and the temperature of the crossflow are set at 3 m/s and 1,200 K, respectively, which closely correspond to the conditions in real boilers. The gas concentration in the crossflow corresponds to the conditions typical of the SNCR process (given in detail in Saario and Oksanen, 2007). The resulting jet to crossflow velocity ratio is 38, which indicates a rather weak crossflow. The concentration of ammonia in the jet is set at 0.66 vol.% and the rest is air. The left and right side boundaries, as well as the boundary opposite the wall that the jet comes from, are defined as symmetry boundaries instead of as open outlets. The heat flux is set at zero on the wall that the jet comes from.

4.3.1 Local grid refinement in reactive jet in crossflow. The baseline, dense, and very dense grids of hexahedral cells are the same as in the axisymmetric case (Table II). The local grid refinement is based on the gradient of velocity magnitude; otherwise the local grid refinement procedure is similar to that described in Section 4.2.1. The details related to the refined grids in the crossflow case are given in the last section of Table II. Of grids I-V of tetrahedral cells summarized in Table III, the grid which turned out to be the best in the axisymmetric case, i.e. grid I, is used in the crossflow case. The dense grid of tetrahedral cells in Table III is the same as in the axisymmetric case.

Grid of hexahedral cells	Total number of cells	Total number of nodes	Local grid refinement criterion	Number of cells at jet inlet
Baseline	102,524	1,095,122	–	4
Dense	2,067,424	1,180,654	–	100
Very dense	4,264,650	346,560	–	169
Nonreactive axisymmetric jet				
Once refined	105,968	113,620	$k > 35\,\mathrm{m}^2/\mathrm{s}^2$	16
Twice refined	109,412	117,869	$k > 211\,\mathrm{m}^2/\mathrm{s}^2$	16
Three times refined	112,856	122,561	$k > 394\,\mathrm{m}^2/\mathrm{s}^2$	16
Nonreactive axisymmetric jet				
Once refined	105,968	114,754	$V^{1/3}\lvert\partial^2 U/\partial x_i \partial x_i\rvert \geq 0.079\ \mathrm{m/s}^2$	16
Twice refined	109,412	119,307	$V^{1/3}\lvert\partial^2 U/\partial x_i \partial x_i\rvert \geq 0.056\ \mathrm{m/s}^2$	52
Three times refined	112,856	124,815	$V^{1/3}\lvert\partial^2 U/\partial x_i \partial x_i\rvert \geq 0.044\ \mathrm{m/s}^2$	52
Reactive jet in crossflow				
Once refined	105,968	115,099	$V^{1/3}\lvert\partial^2 U/\partial x_i \partial x_i\rvert \geq 0.228\ \mathrm{m/s}^2$	16
Twice refined	109,412	120,370	$V^{1/3}\lvert\partial^2 U/\partial x_i \partial x_i\rvert \geq 0.179\ \mathrm{m/s}^2$	28
Three times refined	112,856	125,572	$V^{1/3}\lvert\partial^2 U/\partial x_i \partial x_i\rvert \geq 0.144\ \mathrm{m/s}^2$	28

Notes: Symbol k is turbulence kinetic energy; V is cell volume; and U is mean velocity magnitude

Table II.
Grids of hexahedral cells used in single jet modeling

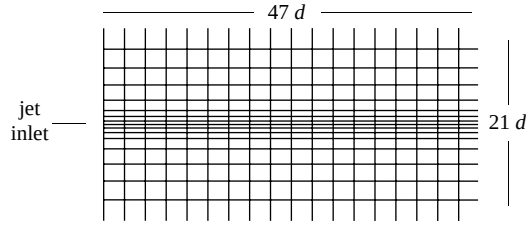

(a) Baseline grid of hexahedral cells (102,524 cells)

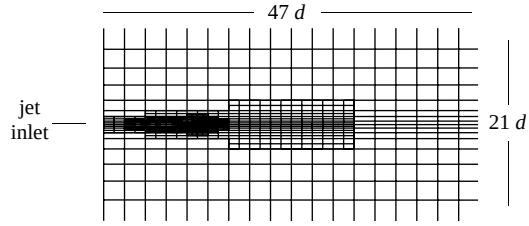

(b) Grid of hexahedral cells after 3rd refinement based on k (112,856 cells)

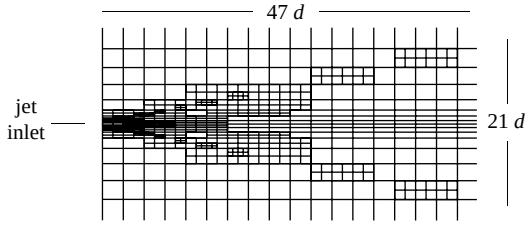

(c) Grid of hexahedral cells after 3rd refinement based on $\partial U / \partial x_i$ (112,856 cells)

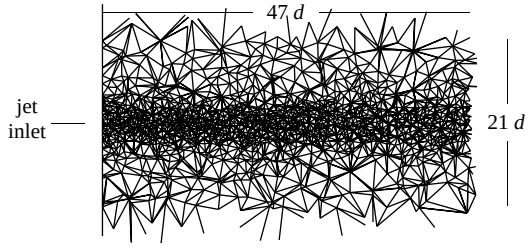

(d) Grid I of tetrahedral cells after (73,994 cells)

Notes: Grids at plane cutting jet axis. See Table II for Figures 2(a)-(c) and Table III for Figure 2(d). Symbol d is jet inlet diameter (42.5 mm)

Figure 2.
Single jet modeling

5. Mathematical modeling

Assuming incompressible steady-state flow, the Favre-averaged (Poinsot and Veynante, 2005, pp. 140-2) continuity and momentum equations can be written as:

$$\frac{\partial}{\partial x_i}(\bar{\rho}\tilde{u}_i) = 0, \tag{2}$$

$$\frac{\partial}{\partial x_i}(\bar{\rho}\tilde{u}_j\tilde{u}_i) = \frac{\partial \bar{p}}{\partial x_i} + \frac{\partial}{\partial x_j}\left[\mu\left(\frac{\partial \tilde{u}_i}{\partial x_j} + \frac{\partial \tilde{u}_j}{\partial x_i} - \frac{2}{3}\,\delta_{ij}\frac{\partial \tilde{u}_l}{\partial x_l}\right)\right] + \bar{\rho}g_i + \frac{\partial}{\partial x_j}(-\bar{\rho}\tilde{u_i''u_j''}), \tag{3}$$

where ρ is density, u_i is the ith component of the velocity vector, p is pressure, μ is viscosity, δ_{ij} is the Kronecker delta, g_i is the ith component of the gravitational vector, and $-\bar{\rho}\tilde{u_i''u_j''}$ is the component of the Reynolds stress tensor. The overbar denotes time-averaging, the tilde denotes Favre-averaging, and the double prime denotes the Favre-averaged fluctuating part.

A part of the grid dependency study is carried out using reactive cases, which require a conservation equation also for energy and equations for the species transport. Moreover, additional sub-models are required. The reactions of ammonia and nitric oxide are modeled using a global mechanism of Duo *et al.* (1992). The turbulence-chemistry interaction is modeled using the eddy dissipation concept of Ertesvag and Magnussen (2000). The finite-volume method (Raithby and Chui, 1990) together with the weighted sum of grey gases model (Smith *et al.*, 1982) are used to model radiative heat transfer. For details on the modeling of the reactive cases the reader is referred to Saario and Oksanen (2007).

5.1 Turbulence modeling

The Reynolds stresses, $-\bar{\rho}\tilde{u_i''u_j''}$, are modeled using widely applied two-equation turbulence models, namely the standard k-ε model (Launder and Spalding, 1972; Launder and Sharma, 1974) and its modification by Shih *et al.* (1995). Reynolds stresses are modeled by invoking the Boussinesq hypothesis, which represents turbulence as an increased viscosity assuming an analogy between the action of viscous stresses and Reynolds stresses on the mean flow:

$$-\bar{\rho}\tilde{u_i''u_j''} = \mu_t\left(\frac{\partial \tilde{u}_i}{\partial x_j} + \frac{\partial \tilde{u}_j}{\partial x_i}\right) - \frac{2}{3}\mu_t\frac{\partial \tilde{u}_l}{\partial x_l}\,\delta_{ij} - \frac{2}{3}\bar{\rho}k\delta_{ij}. \tag{4}$$

In the above equation, k is the turbulence kinetic energy and μ_t is the turbulent viscosity defined as:

Grid of tetrahedral cells	Total number of cells	Total number of nodes	Number of cells at jet inlet	Initial cell size at jet centerline	Cell size growth rate from jet centerline
I	73,994	13,237	14	0.71d	1.45
II	74,306	13,273	14	0.59d	1.46
III	74,526	13,302	14	2.31d	1.20
IV	74,006	13,230	2	0.89d	1.39
V	73,997	13,225	2	0.59d	1.46
Dense	2,067,513	348,794	100	0.12d	1.11

Note: Symbol d is jet inlet diameter (42.5 mm)

Table III.
Grids of tetrahedral cells used in single jet modeling

$$\mu_t = C_\mu \bar{\rho} \frac{k^2}{\varepsilon}, \tag{5}$$

where C_μ is a model constant and ε stands for the dissipation of turbulence kinetic energy. The transport equation for k is written as:

$$\frac{\partial}{\partial x_i}(\bar{\rho}\tilde{u}_i k) = \frac{\partial}{\partial x_i}\left[\left(\mu + \frac{\mu_t}{\sigma_k}\right)\frac{\partial k}{\partial x_i}\right] - \bar{\rho}\tilde{u_i''u_j''}\frac{\partial \tilde{u}_j}{\partial x_i} - g_i\frac{\mu_t}{\bar{\rho}Pr_t}\frac{\partial \bar{\rho}}{\partial x_i} - \bar{\rho}\varepsilon, \tag{6}$$

where the term on the left-hand side represents the convective transfer of k. The first, second, third, and fourth term on the right-hand side represent the diffusive transfer of k, the production of k due to the mean velocity gradients, the production of k due to buoyancy, and the dissipation of k, respectively. Pr_t is the turbulent Prandtl number set at 0.7. The equation for e is empirical instead of being based on exact derivation (Pope, 2000, p. 375), and it is the weakest part of two-equation models (White, 2006, p. 471). The following equation for e is applied (the standard k-ε model):

$$\frac{\partial}{\partial x_i}(\bar{\rho}\tilde{u}_i \varepsilon) = \frac{\partial}{\partial x_i}\left[\left(\mu + \frac{\mu_t}{\sigma_\varepsilon}\right)\frac{\partial \varepsilon}{\partial x_i}\right] - C_1\frac{\varepsilon}{k}\bar{\rho}\tilde{u_i''u_j''}\frac{\partial \tilde{u}_j}{\partial x_i} - C_2\bar{\rho}\frac{\varepsilon^2}{k}, \tag{7}$$

where the term on the left-hand side represents the convective transfer of ε. The first, second, and third term on the right-hand side represent the diffusive transfer of ε, the production of ε, and the dissipation of ε, respectively. The model constants in equations (5)-(7) are based on Launder and Sharma (1974): $C_\mu = 0.09$, $\sigma_k = 1.0$, $\sigma_\varepsilon = 1.3$, $C_1 = 1.44$, and $C_2 = 1.92$.

In the k-ε model of Shih *et al.* (1995), equation (6) for k remains unchanged. The ε equation formulation is based on the equation of the mean-square vorticity fluctuation and reads:

$$\frac{\partial}{\partial x_i}(\bar{\rho}\tilde{u}_i \varepsilon) = \frac{\partial}{\partial x_i}\left[\left(\mu + \frac{\mu_t}{\sigma_\varepsilon}\right)\frac{\partial \varepsilon}{\partial x_i}\right] - C_1\bar{\rho}S\varepsilon - C_2\bar{\rho}\frac{\varepsilon^2}{k + \sqrt{v\varepsilon}}. \tag{8}$$

The main difference with respect to the standard k-ε model dissipation equation (equation (7)) is the production term. C_1 in equation (8) is a variable defined as:

$$C_1 = \max\left\{0.43, \frac{Sk/\varepsilon}{5 + Sk/\varepsilon}\right\}, \tag{9}$$

where S stands for the mean strain rate defined by the following two expressions:

$$S = \sqrt{2S_{ij}S_{ij}},\ S_{ij} = \frac{1}{2}\left(\frac{\partial \tilde{u}_i}{\partial x_j} + \frac{\partial \tilde{u}_j}{\partial x_i}\right). \tag{10}$$

In addition to the differences in the ε equation, $C\mu$ in equation (5) is no longer constant, but is made variable based on the realizability conditions (Shih *et al.*, 1995):

$$C_\mu = \frac{1}{A_0 + A_s\mu^*\frac{k}{\varepsilon}}. \tag{11}$$

Constant A_0 was set at 4.04, and the parameter $A_s = \sqrt{6}\cos\phi$, where:

$$\phi = \frac{1}{3}\cos^{-1}\left(\sqrt{6}\frac{S_{ij}S_{jk}S_{ki}}{\left(\sqrt{S_{ij}S_{ij}}\right)^3}\right). \tag{12}$$

In equation (11) u^* is defined by the following expressions:

$$u^* = \sqrt{S_{ij}S_{ij} + \tilde{\Omega}_{ij}\tilde{\Omega}_{ij}}, \quad \tilde{\Omega}_{ij} = \Omega_{ij} = \bar{\Omega}_{ij} - \varepsilon_{ijk}\omega_k, \tag{13}$$

where ε_{ijk} is the alternating symbol (Levi-Civita symbol) and $\bar{\Omega}_{ij}$ is the mean rotation rate viewed in a rotating reference frame with the angular velocity ω_k. According to Shih *et al.* (1995), their definition corresponds better to the experimentally observed values of C_μ in a variety of flows. The remaining model constants were calibrated with respect to basic flow configurations: $\sigma_k = 1.0$, $\sigma_\varepsilon = 1.2$, and $C_2 = 1.9$.

The turbulence intensity at the jet inlet, I, is calculated as follows:

$$I = \frac{u'}{u_0} = 0.16(Re_d)^{-1/8}, \tag{14}$$

where u' is the fluctuating velocity, u_0 is the jet inlet velocity, and d denotes the jet inlet (hydraulic) diameter. The turbulence kinetic energy, k, and its dissipation, ε, at the jet inlet are obtained from the following relations:

$$k = \frac{3}{2}(u_0 I)^2, \quad \varepsilon = C_\mu^{3/4}\frac{k^{3/4}}{d}. \tag{15}$$

5.2 Numerical solution

Although frequently not referred to in industrial combustion modeling, it is generally known that the chosen numerical scheme may have a significant influence on predictions. This fact is supported by the authors' own experience and has also been demonstrated in Knaus *et al.* (2001). In the present study, a commercial finite-volume-based CFD solver Fluent Inc. (2005) is used to solve discretized equations. There are two advantageous features in finite-volume methods: physically, the conservation of mass, momentum, and energy is assured in the formulation itself and, numerically, unstructured grids and arbitrary geometries are accommodated without coordinate transformation (Chung, 2002, p. 239). Fluent applies an unstructured grid solver, which cannot exploit all the benefits related to grids of hexahedral cells.

The discretized equations are solved using the Gauss-Seidel method together with the algebraic multigrid approach. The pressure field is calculated from the continuity equation using the SIMPLE algorithm. The discretization of convective terms is performed applying a second-order accurate upwinding scheme. The values at the faces of computational cells, $\tilde{\phi}_f$ are obtained from (Murthy and Mathur, 2001):

$$\tilde{\phi}_f = \tilde{\phi}_0 + \frac{\partial\tilde{\phi}}{\partial x_i}\cdot\Delta\mathbf{s}, \tag{16}$$

where $\tilde{\phi}_0$ is the cell center value in the upstream cell and $\mathbf{s}$ is the displacement vector from the upstream cell center to the face. A second-order central difference discretization scheme is used for the diffusion terms. The gradient $\partial\tilde{\phi}/\partial x_i$ in the diffusion terms, as well as in equation (16), is defined using the Gauss theorem:

$$\frac{\partial \tilde{\phi}}{\partial x_i} = \frac{1}{V}\sum_{f=1}^{F} \tilde{\phi}_{f,2} A_f, \tag{17}$$

where subscript f denotes face, A_f is the cell face area, and F is the number of faces enclosing the cell. In equation (17), $\tilde{\phi}_{f,2}$ is computed from:

$$\tilde{\phi}_{f,2} = \frac{1}{N}\sum_{n=1}^{N} \tilde{\phi}_n, \tag{18}$$

where N is the number of nodes on the face, subscript n denotes node, and the nodal values $\tilde{\phi}_n$ are constructed from the weighted average of the cell center values surrounding the nodes. The pressure at the face of the computational cell is obtained using linear interpolation between adjacent cell center values.

6. Results and discussion

6.1 Full boiler

Obtaining a strictly converged and stabilized steady solution in industrial boiler modeling is sometimes difficult, which may be due to the complicated system of equations and models. Hence, it is of importance to try to assess the magnitude of iteration error. The iteration error and the grid dependency of the full boiler model are studied by plotting the vertical velocity component, u_z, along line A located at: $x = 4.6\,\text{m}$, $z = 8.0\,\text{m}$ (Figure 1(a)).

Figure 3(a) shows that the iteration error has not been completely removed from the solution. Here, the under-relaxation factors are set at very low values (below 0.01).

The results differ clearly with different grids, as shown in Figure 3(b). A consistent trend as a function of refined grids cannot be observed. Partially this may be attributed to the fact that all grids, including the dense one, are still rather coarse, considering the huge size of the industrial boiler. Although the iteration error in Figure 3(a) seems smaller than the discretization error in Figure 3(b), the iteration error nevertheless is great enough to render the interpretation of results in Figure 3(b) difficult. Moreover, as a result of the iteration and the discretization errors, it is difficult to judge any errors related to the submodels.

6.2 Nonreactive axisymmetric jet exhausting into quiescent atmosphere

The geometry and conditions of the nonreactive axisymmetric jet were summarized in Section 4.2. The grids applied were summarized in Tables II and III, and some of them were shown in Figure 2. Dimensionless mean axial velocity or dimensionless turbulence kinetic energy are plotted in the following figures, where u, d, x, and r are the mean axial velocity, the jet inlet diameter, the axial distance from the jet inlet, and the radial distance from the jet centerline, respectively, and subscripts 0 and c denote the inlet value and the centerline value, respectively. Let us recall that the modeled jet exhausts into free surroundings (no confining walls). All the results shown below are free of iteration error.

Figures 4 and 5 show that the predictions obtained with the dense grid consisting of 2,067,424 hexahedral cells are not yet perfectly grid-independent (recall that although most of the cells are packed in the jet-like part of the flow, a great number of cells are

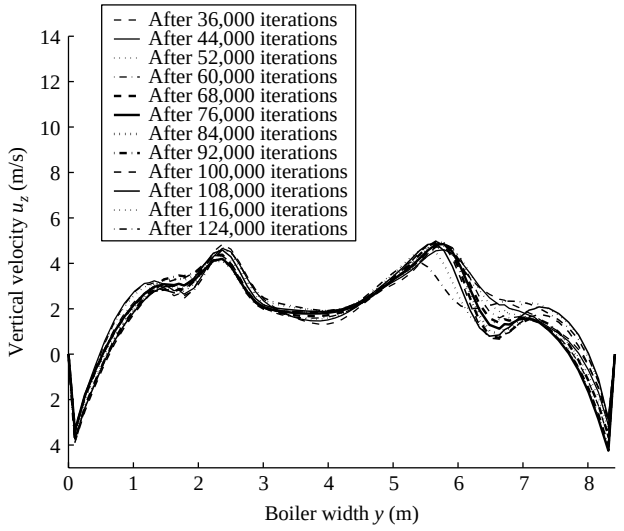

(a) Iteration error with coarse grid (256,654 cells)

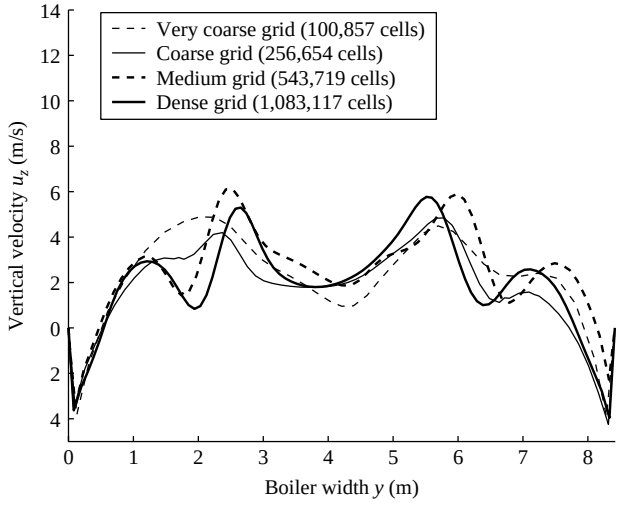

(b) Discretization error (effect of grid refinement)

Note: Vertical velocity uz plotted along line A (see Figure 1(a))

Figure 3.
Iteration and discretization errors in full boiler modeling

still located outside the actual jet). Slight differences can be observed when the predictions of the dense grid are compared with those of the very dense grid of 4,264,650 hexahedral cells. The difference in predictions between dense and very dense grids is rather moderate, and consequently the predictions obtained with the very dense grid can be assumed to approach the grid-independent solution.

In general, a consistent improvement can be observed in predictions in cases where the grid is refined locally several times (Figures 4 and 5). However, it must be noted

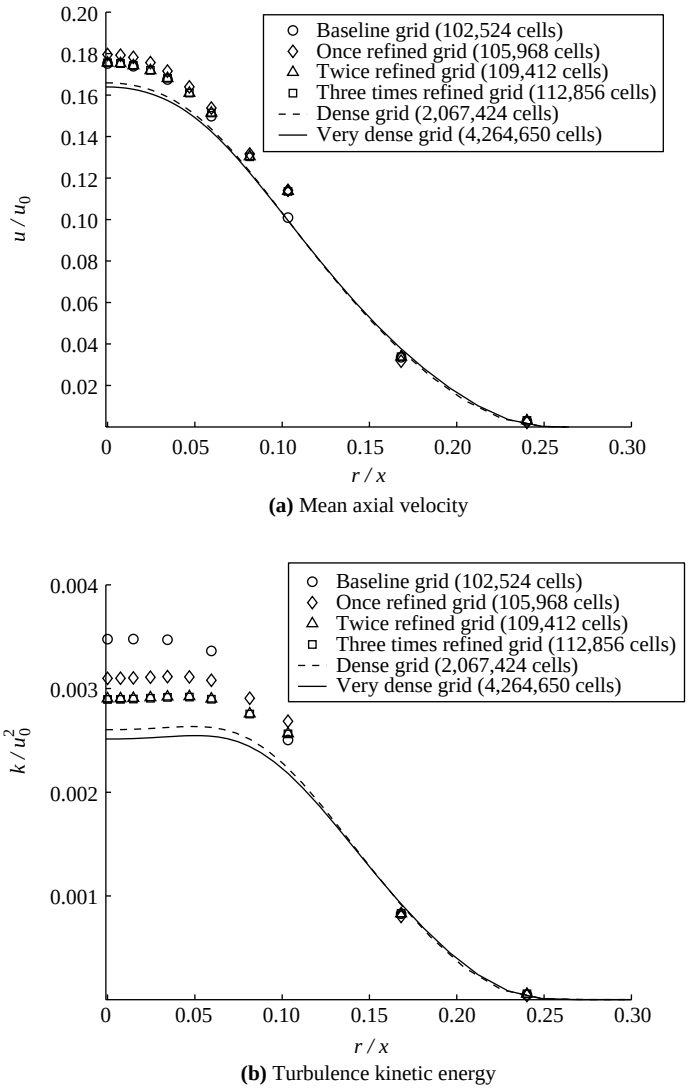

Figure 4.
Effect of local grid refinement with grids of hexahedral cells at $x/d = 30$

Note: Grid refinement based on k, see also Table II

that, depending on the chosen location for presenting the results, the predictions obtained with the baseline grid may even look better than those after the first refinement. Comparing Figures 4(a) and 4(b) shows that the percentual error in the predictions is greater for the turbulence kinetic energy than for the mean axial velocity. This fact is relevant from the point of view of several turbulence-chemistry interaction models in which k directly enters the reaction rate expressions. Figure 4 shows that both u and k are overpredicted near the jet centerline when coarse grids of hexahedral

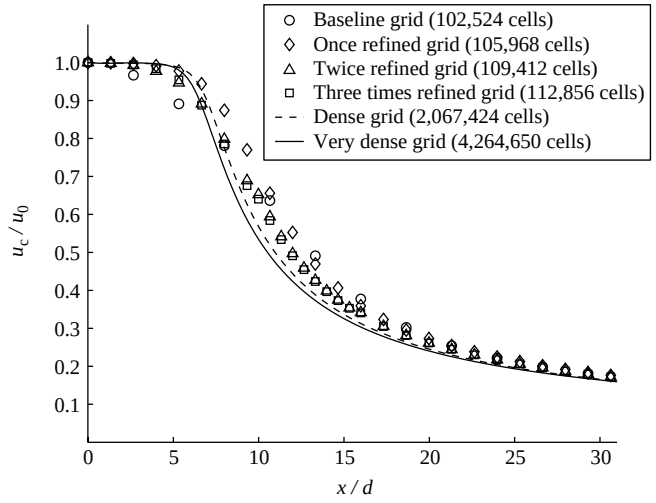

(a) x / d = 0 ... 30

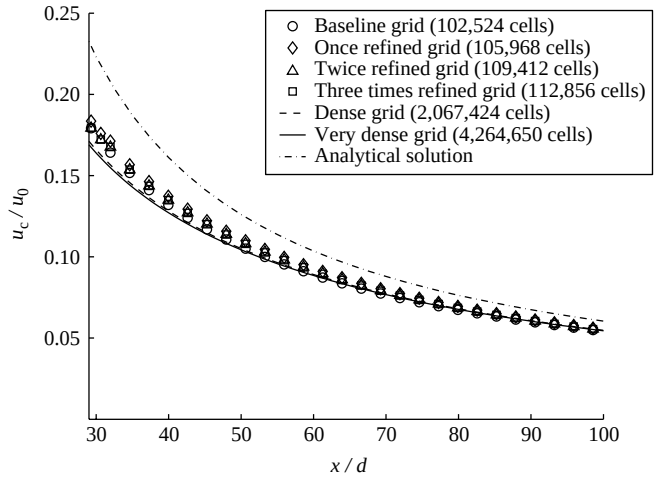

(b) x / d = 30 ... 100

Note: Grid refinement based on k. See also Table II

Figure 5.
Effect of local grid refinement with grids of hexahedral cells

cells are used. It is also observed that the third local grid refinement does not improve significantly the predictions obtained after two local grid refinements.

Analytically calculated centerline velocity, u_c, (using $x_0 = 4$ and $B = 5.8$ in equation (1) on the basis of experiments of Hussein *et al.* (1994, p. 44)) is included in Figure 5(b) in order to assess the possibility of approximating u_c without computer modeling. The jet inlet parameters (d, u_0, and Re) are roughly twice as large in the present study compared to those in Hussein *et al.* (1994, p. 34), in other words they are of the same order in both studies. Moreover, the modeled inlet velocity profile is of plug-flow type, which is nearly the case also in measurements (Hussein *et al.*, 1994, p. 34).

Here, the analytical solution is found to give greater values for u_c than the modeling. This may partially be due to the constants x_0 and B, for which different studies have proposed somewhat different values (Pope, 2000, p. 101; Panchapakesan and Lumley, 1993, p. 204), and also the jet inlet profile and Re might affect x_0 and B (Hussein *et al.*, 1994, pp. 33, 42). Smaller values of x_0 and B would have given a closer match between the analytical solution and the CFD predictions. The difference in the inlet turbulence intensity in measurements and modeling as well as the effect of turbulence models and turbulence anisotropy (not taken into account by k-ε models) may contribute to the observed discrepancy. The trend of mean axial velocity decay is reasonably similar in both the modeling and the analytical solution, although estimating u_c here on the basis of the analytical solution leads to a different result than on the basis of modeling.

Although the turbulence kinetic energy and the velocity gradient are closely interconnected through the production term in equation (6), the grids are clearly different depending on whether the local grid refinement is based on k or $\partial U/\partial x_i$ (Figure 2(b) and 2(c)). Figure 6 shows that also the corresponding predictions are different. In both cases the predictions improve consistently when the grid is refined, and the already mentioned observation of negligible improvement after the third local grid refinement is confirmed as well. The number of cells at the inlet increases more quickly when the refinement is based on $\partial U/\partial x_i$ (Table II and Figure 2(a)-2(c)). It is quite difficult to say reliably which is the better choice, since near the jet axis the refinement based on $\partial U/\partial x_i$ approaches the grid-independent solution more quickly, whereas near the jet edge the refinement based on k is in better agreement with the grid-independent solution. All in all, the results from several locations and as a function of different variables (not shown here) suggest that the refinement based on $\partial U/\partial x_i$ performs slightly better.

The sensitivity of the solution for inlet turbulence intensity is estimated by doubling and halving the inlet intensity used in the reference case ($I = 3.6$ percent). The effect is clear near the inlet, but further away in the self-similar region it is hardly noticeable (Figure 7). The maximum predicted value of k is not much affected by the chosen inlet values. This is explained by the fact that the production of k in the jet shear layer is the dominating factor. Moreover, the high values of k near the jet inlet in the case of doubled turbulence inlet intensity are quickly balanced by the correspondingly high values of ε (equations (6) and (15)). Although not shown here, the effect of inlet turbulence intensity is clearly smaller on the predicted u than on k.

The development of self-similar profiles is shown in Figure 8. The profiles are clearly not self-similar at $x/d < 30$, and the self-similarity of the mean velocity seems to be achieved approximately at $x/d > 50$ (Figure 8(a)). Turbulence kinetic energy seems to achieve self-similarity almost at the same distance as the mean axial velocity; at most only a slight delay can be observed (Figure 8(b)).

Figure 9 shows that the standard k-ε model predicts a greater jet spreading rate than the k-ε model of Shih *et al.* (1995). Hence, the latter model might be a better choice in boiler modeling, as it can provide a better prediction of the jet penetration. However, it should be noted that the turbulence model affects also the predicted reaction rates. Figure 9 closely resembles the result obtained in Shih *et al.* (1995, p. 233). Here, the predictions are not compared with measurements, but these comparisons can be found in Shih *et al.* (1995, p. 233), where it is shown that the k-ε model of Shih *et al.* better predicts the axisymmetric jet spreading rate than the standard k-ε model.

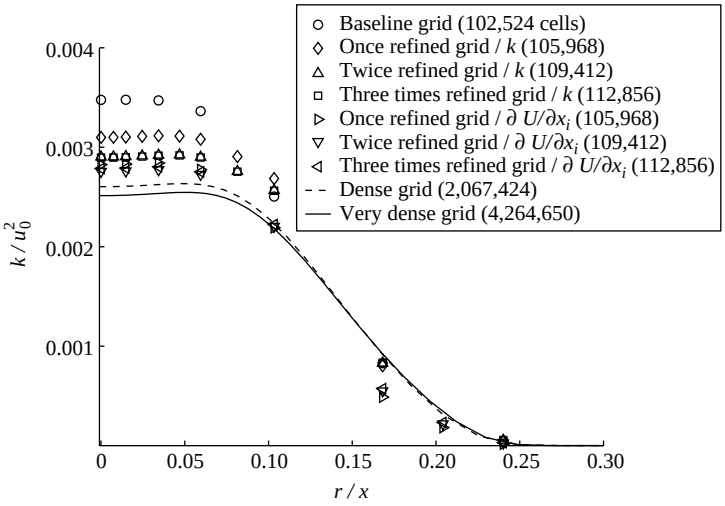

Note: Grid refinement criterion with grids of hexahedral cells at x/d=30. Grid refinement based on k or on $\partial U/\partial x_i$, see also Table II

Figure 6.
Effect of local grid refinement criterion with grids of hexahedral cells at $x/d = 30$

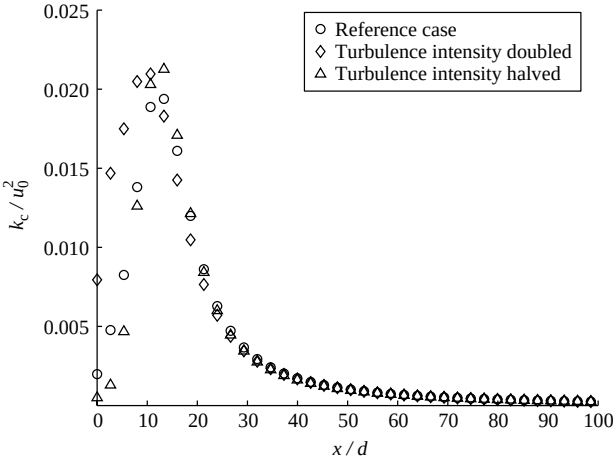

Note: Baseline grid with 102 524 cells

Figure 7.
Sensitivity to turbulence intensity at jet inlet

Figure 10 shows different grids of tetrahedral cells and shows that only the predictions obtained with the dense grid of tetrahedral cells are close to the grid-independent solution. All the other differently generated grids of tetrahedral cells seriously underpredict the jet centerline velocity and overpredict the jet spreading rate. The worst predictions (grid III) have little, if anything, to do with the grid-independent solution. The grid generation technique is of importance in the generation of grids of tetrahedral cells; especially too large an initial cell size at the jet centerline or too few cells at the jet inlet are detrimental for the solution accuracy and may even prevent obtaining a converged solution. In fact, a converged solution was not obtained for grid *V* (not included in Figure 10).

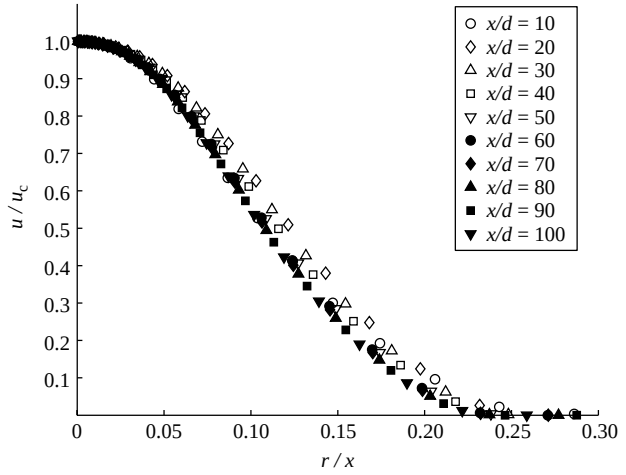

(a) Mean axial velocity

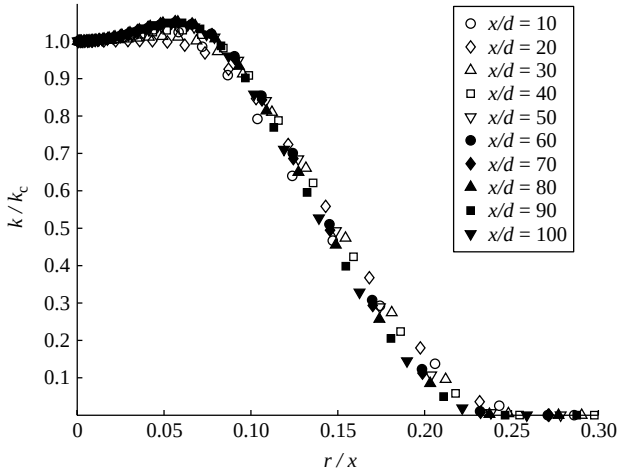

(b) Turbulence kinetic energy

Note: Very dense grid with 4,264,650 cells (every second data point shown)

Figure 8.
Jet self-similarity

It is in the face fluxes where the performance of the cell types differs essentially. The effect of cell types can be assessed on the basis of Figures 4(a), 5, and 10. The baseline grid of hexahedral cells seems to be superior to coarse grids of tetrahedral cells. However, Tables II and III reveal that in a grid consisting of a certain fixed number of cells the number of nodes is clearly smaller in a grid of tetrahedral cells than in a grid of hexahedral cells. Hence, a comparison based on a similar number of nodes instead of on a similar number of cells would lead to an improved performance of grids of tetrahedral cells with respect to grids of hexahedral cells.

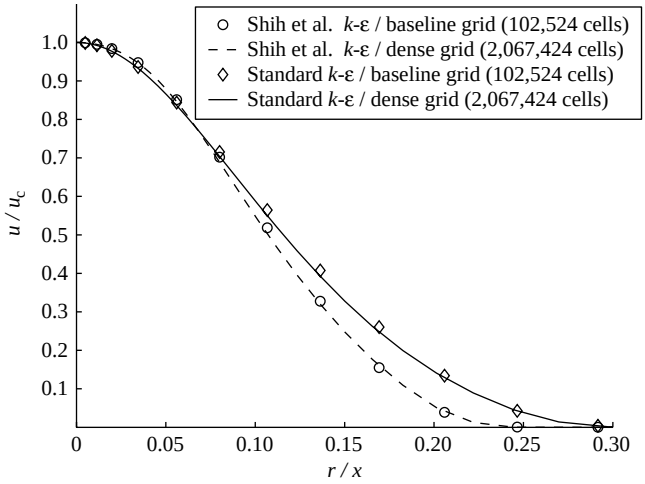

Figure 9.
Mean axial velocity profiles with Shih *et al.* and standard k-ε models at $x/d = 90$

6.3 Reactive jet exhausting into crossflow

Figure 11 shows the predicted jet penetration into crossflow as a function of axial distance. Figure 12 shows the predicted velocity magnitude and ammonia concentration at $x/d = 60$ where significant jet bending has occurred. Figure 13 shows the predicted rate of reaction $NH_3 + NO \rightarrow N_2 + H_2O + (1/2)H_2$ and temperature at $x/d = 30$.

As in the axisymmetric case, it can be observed that the predictions obtained with the dense grid consisting of 2,067,424 hexahedral cells are not perfectly grid-independent, although the difference between the dense and very dense grids is almost negligible. Moreover, consistent with the findings of the axisymmetric jet modeling, the following observations can be made. The local grid refinement provides a consistent improvement in predictions. The third local grid refinement does not improve significantly the predictions obtained after two local grid refinements. Grid I of tetrahedral cells underpredicts the jet centerline velocity and the jet penetration, whereas the baseline grid of hexahedral cells does the opposite (Figures 11 and 12(a)). Grid I of tetrahedral cells overpredicts the jet spreading rate (Figure 12(a)). Although not shown in the figures, it is also confirmed that the percentual error in the predictions is generally either of the same magnitude or slightly greater for the turbulence kinetic energy than for the mean velocity magnitude.

In general, unlike in the axisymmetric case, it can be observed that the baseline grid of hexahedral cells performs as badly as grid I of tetrahedral cells. This finding can be partially attributed to the fact that the hexahedral cells with a large edge ratio perform poorly when the flow is not aligned with the grid lines, which is the case in crossflow. It should be noted also that in the crossflow case the region of densest grid does not follow the trajectory of the bending jet.

The discrepancies in the predictions of velocity magnitude and ammonia concentration are consistent with each other and of the same magnitude, as shown in Figure 12. Figure 13(a) shows that near the jet inlet ($x/d = 30$) the reaction rate is highest in the jet shear layer and that the reaction rates are greater on the wind side of the jet. Lower reaction rates near the jet centerline are explained mainly by the lower temperature there (compare

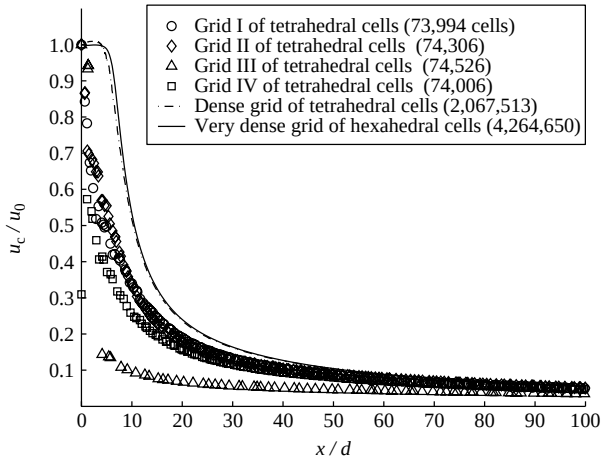

(a) $x / d = 0 \ldots 100$ (every third data point shown)

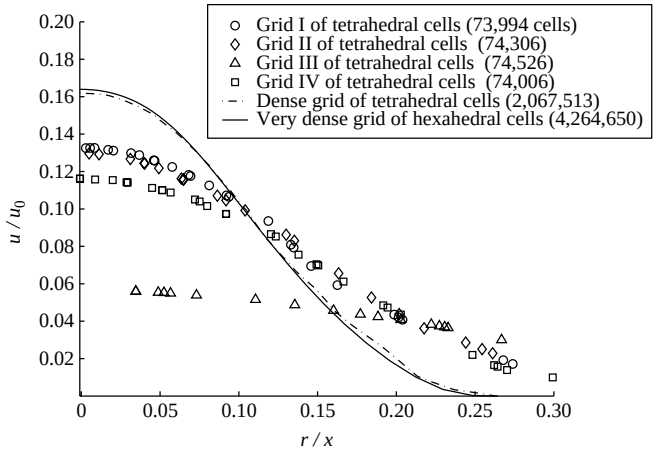

(b) $x / d = 30$

Figure 10.
Mean axial velocities using differently generated grids of tetrahedral cells and very dense grid of hexahedral cells

Figure 13(a) and 13(b)). Proceeding to downwind, the temperature and the concentration of nitric oxide increase in the jet centerline due to turbulent mixing. Consequently, downwind ($x/d > 60$) the reaction rates are no longer greatest in the jet shear layer; instead the reaction rate increases towards the jet centerline (not shown in Figure 13).

In general, errors observed in the predictions of reaction rate and of reactive species concentrations are a consequence of the erroneous prediction of the flow field. Here, the heat release from the reactions of ammonia is almost negligible due to the low-ammonia concentration. It is assumed that the errors related to the prediction of reactive flow would have been even greater if the heat release had been significant, as is the case in the combustion of solid, liquid, and gaseous fuels.

It must be noted that the crossflow velocity profile in a real boiler is not of the plug-flow type. As Figure 3 reveals, real jets may even encounter strong downward

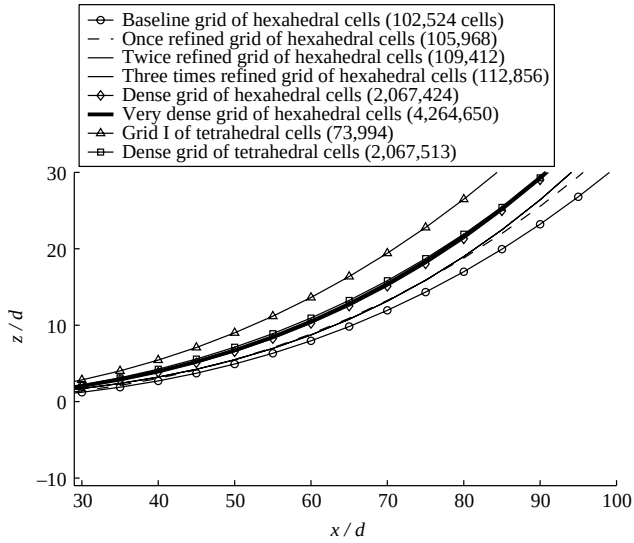

Notes: Trajectories based on maximum velocity. Grid refinement based on du/dx_i . Note that trajectories of twice and three times refined grids are identical.See also Tables II and III

Figure 11.
Jet penetrating into crossflow

velocity components near the walls of the boiler. Also, it must be noted that stronger crossflow (or weaker jet) could have produced somewhat different results, so that the results obtained here should be considered valid only for jets exhausting into a weak crossflow.

7. Conclusions

In industrial-scale boiler modeling a bad quality computational grid may cause a greater error in the predictions than the turbulence and other models used. The present study emphasizes the fact that the grid dependency study is an essential part of every modeling study and that the discretization error should be minimized, or at least assessed, if any definite conclusions are to be drawn from the results. Obtaining a perfectly grid-independent solution in industrial-scale reactive flow modeling in a reasonable time is beyond the ability of current standard computers.

First, several grids of hexahedral cells covering the full boiler volume are generated to show the difficulties related to judging iteration, discretization, and modeling errors in boiler modeling. In the second stage, studies with a single jet exhausting both into a quiescent atmosphere and into a weak crossflow are carried out to provide information for local grid refinement at critical parts of the boiler (near jets).

It is found that, strictly speaking, over four million computational cells are required for a single jet to obtain the grid-independent solution. However, judging somewhat less strictly, it can be concluded that using approximately two million cells gives a reasonably grid-independent solution for a single jet both with grids of hexahedral and tetrahedral cells. It must be noted that the above absolute numbers of cells are somewhat misleading indicators since not all cells are located in the jet-like part of the flow. The local grid refinement provides a significant improvement in the predictions

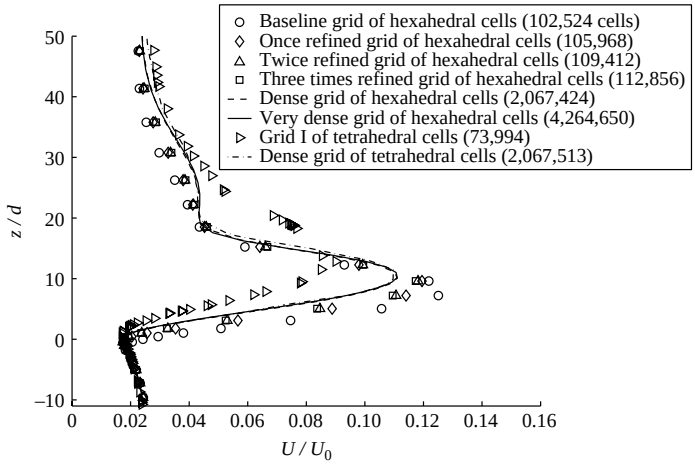

(a) Mean velocity magnitude at $x / d = 60$

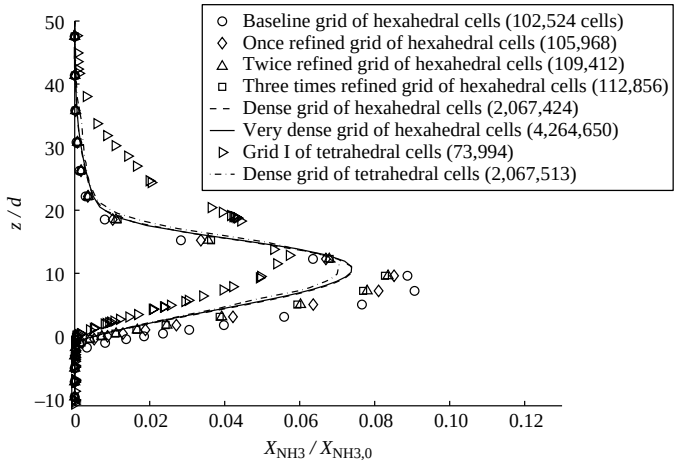

(b) Ammonia concentration at $x / d = 60$

Note: Grid refinement based on $\partial ll/\partial x_i$. See also Tables II and III.

Figure 12.
Jet penetrating into crossflow

with a relatively low increase in the number of cells and computer time. Here, refining the grid locally twice near the jets is sufficient to obtain a significant improvement. Moreover, in the axisymmetric jet case, refinement based on the velocity gradient performs slightly better than that based on the turbulence kinetic energy.

It is shown that a finite-volume-based solver with a relatively coarse grid of tetrahedral cells, as typically used in industrial boiler modeling, may cause serious errors unless the grid is generated with care and using a sufficient number of cells. The jet spreading rate is strongly overpredicted and the mean centerline velocity is strongly underpredicted with coarse grids of tetrahedral cells. Conversely, relatively coarse grids of hexahedral cells overpredict the mean centerline velocity. The spreading rate of axisymmetric jet is reasonably well predicted with coarse grids of hexahedral cells.

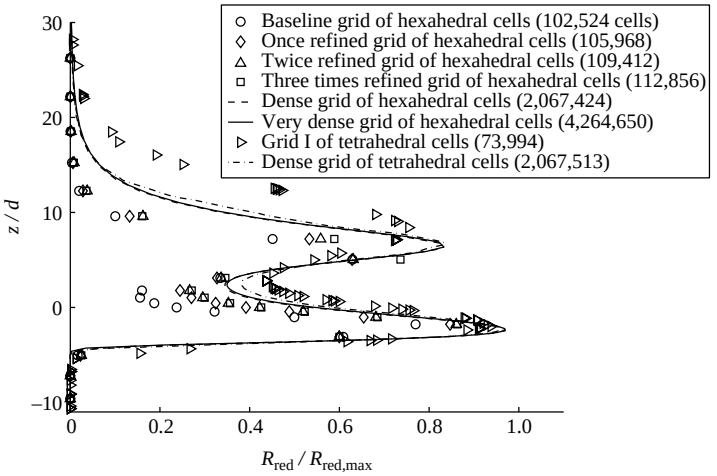

(a) Rate of reaction $NH_3 + NO \rightarrow N_2 + H_2O + 1/2\ H_2$ at $x / d = 30$

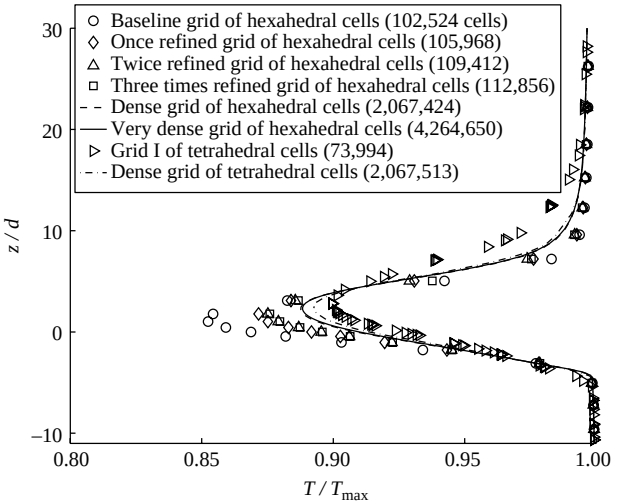

(b) Temperature at $x / d = 30$

Notes: Symbols $R_{red,max}$ and T_{max} correspond to maximum values obtained with very dense grid of hexahedral cells. Grid refinement based on $\partial U/\partial x_i$, see also Tables II and III

Figure 13.
Jet penetrating into crossflow

In general, the quality of predictions obtained with grids of hexahedral cells deteriorates in the crossflow case, where the flow is not aligned with the grid lines. The differences in the predictions are significant when the chemical reactions are taken into account.

The comparison of two turbulence models shows that the k-ε model of Shih *et al.* (1995) predicts a lower axisymmetric jet spreading rate than the standard k-ε model,

which is a result consistent with the literature. The uncertainty in estimated turbulence intensity at the jet inlet is probably not among the most critical error sources. Finally, the predicted centerline velocity-decay trend of an axisymmetric jet is shown to be reasonably similar to that based on the analytical correlation, but the absolute values are not the same.

References

Andreopoulos, J. and Rodi, W. (1984), "Experimental investigation of jets in a crossflow", *Journal of Fluid Mechanics*, Vol. 138, pp. 93-127.

Casey, M. and Wintergerste, T. (Eds) (2000), *Special Interest Group on "Quality and Trust in Industrial CFD": Best Practice Guidelines*, European Research Community on Flow, Turbulence and Combustion (ERCOFTAC), Version 1.0.

Chung, T.J. (2002), *Computational Fluid Dynamics*, Cambridge University Press, Cambridge.

Coelho, P.J. and Carvalho, M.G. (1996), "Evaluation of a three-dimensional mathematical model of a power station boiler", *Journal of Gas Turbines and Power-Transactions of the ASME*, Vol. 118, pp. 887-95.

Duo, W., Dam-Johansen, K. and Ostergaard, K. (1992), "Kinetics of the gas-phase reaction between nitric oxide, ammonia and oxygen", *Canadian Journal of Chemical Engineering*, Vol. 70, pp. 1014-20.

Ertesvag, I.S. and Magnussen, B.F. (2000), "The eddy dissipation turbulence energy cascade model", *Combustion Science and Technology*, Vol. 159, pp. 213-35.

Ferziger, J. and Peric, M. (1999), *Computational Methods for Fluid Dynamics*, Springer-Verlag, Berlin.

Fluent Inc. (2005), *Fluent 6.2. User's Guide*, available at: www.fluent.com

Gillis, P.A. and Smith, P.J. (1990), "An evaluation of three-dimensional computational combustion and fluid-dynamics for industrial furnace geometries", *Proceedings of the Combustion Institute*, Vol. 23, pp. 981-91.

Hill, S.C. and Smoot, L.D. (2000), "Modeling of nitrogen oxides formation and destruction in combustion systems", *Progress in Energy and Combustion Science*, Vol. 26, pp. 417-58.

Hussein, H.J., Capp, S. and George, W.K. (1994), "Velocity measurements in a high-Reynolds-number, momentum-conserving, axisymmetric, turbulent jet", *Journal of Fluid Mechanics*, Vol. 258, pp. 31-75.

Karvinen, A. and Ahlstedt, H. (2005), "Comparison of turbulence models in case of jet in crossflow using commercial CFD code", in Rodi, W. and Mulas, M. (Eds), *Engineering Turbulence Modelling and Experiments*, Vol. 6, Elsevier, Amsterdam.

Karvinen, A., Ahlstedt, H., Ala-Juusela, J., Hellsten, A. and Huhtanen, R. (2006), "Effects of grid density and turbulence models on a jet in crossflow", paper presented at 7th European Conference on Industrial Furnaces and Boilers, Oporto, April 18-21.

Knaus, H., Schnell, U. and Hein, K.R.G. (2001), "Evaluation of the 3-D furnace simulation code AIOLOS by comparing CFD predictions of gas compositions with in-furnace measurements in a 210 MW coal-fired utility boiler", *Progress in Computational Fluid Dynamics*, Vol. 1, pp. 62-9.

Launder, B.E. and Sharma, B.I. (1974), "Application of the energy-dissipation model of turbulence to the calculation of flow near a spinning disc", *Letters in Heat and Mass Transfer*, Vol. 1, pp. 131-8.

Launder, B.E. and Spalding, D.B. (1972), *Lectures in Mathematical Models of Turbulence*, Academic Press, Boston, MA.

Lockwood, F.C., Abbas, T., Kandamby, N.H. and Sakthitharan, V. (2001), "CFD experience on industrial combustors", *Progress in Computational Fluid Dynamics*, Vol. 1, pp. 1-13.

Miller, J.A. and Bowman, C.T. (1989), "Mechanism and modeling of nitrogen chemistry in combustion", *Progress in Energy and Combustion Science*, Vol. 15, pp. 287-338.

Murthy, J.Y. and Mathur, S.R. (2001), "Unstructured mesh methods for combustion problems", in Baukal, C.E., Gershtein, V.Y. and Li, X. (Eds), *Computational Fluid Dynamics in Industrial Combustion*, CRC Press, Boca Raton, FL.

Panchapakesan, N.R. and Lumley, J.L. (1993), "Turbulence measurements in axisymmetric jets of air and helium. Part 1. Air jet", *Journal of Fluid Mechanics*, Vol. 246, pp. 197-223.

Poinsot, T. and Veynante, D. (2005), *Theoretical and Numerical Combustion*, 2nd ed., R.T. Edwards, Philadelphia, PA.

Pokela, H. and Huttunen, M. (2005), "Laskentaverkkotarkasteluita polton tarkempaa mallinnusta varten soodakattilassa", Report PRO5/P5023/05, VTT Technical Research Centre of Finland (in Finnish).

Pope, S.B. (2000), *Turbulent Flows*, Cambridge University Press, Cambridge.

Raithby, G.D. and Chui, E.H. (1990), "A finite-volume method for predicting a radiant heat transfer in enclosures with participating media", *Journal of Heat Transfer-transactions of the ASME*, Vol. 112, pp. 415-23.

Roache, P.J. (1994), "Perspective: a method for uniform reporting of grid refinement studies", *Journal of Fluids Engineering-transactions of the ASME*, Vol. 116, pp. 405-13.

Saario, A. and Oksanen, A. (2007), "Comparison of global ammonia chemistry mechanisms in biomass combustion and selective noncatalytic reduction process conditions", *Energy and Fuels*, Vol. 21 No. 1.

Shih, T-H., Liou, W.W., Shabbir, A., Yang, Z. and Zhu, J. (1995), "A new k-ε eddy viscosity model for high Reynolds number turbulent flows", *Computers & Fluids*, Vol. 24, pp. 227-38.

Smith, T.F., Shen, Z.F. and Friedman, J.N. (1982), "Evaluation of coefficients for the weighted sum of gray gases model", *Journal of Heat Transfer-transactions of the ASME*, Vol. 104, pp. 602-8.

Stopford, P.J. (2002), "Recent applications of CFD modeling in the power generation and combustion industries", *Applied Mathematical Modeling*, Vol. 26, pp. 351-74.

Weber, R., Peters, A.A.F., Breithaupt, P.P. and Visser, B.M. (1993), "What can combustion engineers expect from modeling? Pulverized coal combustion through swirl burners", *ASME FACT*, Vol. 17, pp. 71-86.

Weber, R., Wecel, G., Verlaan, A., Breussin, F. and Dugué, J. (1998), "Experimental and numerical studies on reburn jet penetration and mixing with application to boilers and municipal waste incinerators", *Journal of the Institute of Energy*, Vol. 71, pp. 94-109.

White, F.M. (2006), *Viscous Fluid Flow*, McGraw-Hill, New York, NY.

Wilcox, D.C. (1998), *Turbulence Modeling for CFD*, DCW Industries, La Cañada, CA.

Corresponding author
A. Saario can be contacted at: ari.saario@tut.fi